Iridium/GPS Carrier Phase Positioning and Fault Detection Over Wide Areas

Mathieu Joerger, Jason Neale and Boris Pervan, *Illinois Institute of Technology*

BIOGRAPHY

Dr. Mathieu Joerger obtained a Master in Mechatronics from the National Institute of Applied Sciences in Strasbourg, France, in 2002. He pursued studies in Mechanical and Aerospace Engineering at the Illinois Institute of Technology (IIT) in Chicago, where he earned a M.S. degree in 2002, and a Ph.D. in 2009. His topics of research included autonomous ground vehicle navigation and control, integration of GPS with laser-scanners, and augmentation of GPS using carrier phase measurements from low-earth-orbit telecommunication satellites. He is currently working as a research associate at IIT on multi-constellation navigation satellite systems for high-integrity precision applications.

Jason Neale is a Master's degree candidate at the Illinois Institute of Technology. His work focuses on modeling the ionosphere with various levels of geomagnetic activity for use in iGPS applications. Jason received his bachelor's degree in aerospace engineering from the Illinois Institute of Technology in 2007.

Dr. Boris Pervan is Associate Professor of Mechanical and Aerospace Engineering at the Illinois Institute of Technology (IIT), where he conducts research on high-integrity satellite navigation systems. Prof. Pervan received his B.S. from the University of Notre Dame, M.S. from the California Institute of Technology, and Ph.D. from Stanford University. Prior to joining the faculty at IIT, he was a spacecraft mission analyst at Hughes Space and Communications Group and was project leader at Stanford University for GPS LAAS research and development. He was the recipient of the Mechanical and Aerospace Dept. Excellence in Research Award (2007), IIT/Sigma Xi Excellence in University Research Award (2005), University Excellence in Teaching Award (2005), Ralph Barnett Mechanical and Aerospace Dept. Outstanding Teaching Award (2002, 2009), IEEE Aerospace and Electronic Systems Society M. Barry Carlton Award (1999), RTCA William E. Jackson Award (1996), Guggenheim Fellowship (Caltech 1987), and Albert J. Zahm Prize in Aeronautics (Notre Dame 1986). He is currently Editor of the ION journal Navigation.

ABSTRACT

The iGPS high-integrity precision navigation system combines carrier phase ranging measurements from GPS and low earth orbit Iridium telecommunication satellites. Large geometry variations generated by fast moving Iridium spacecraft enable the rapid floating estimation of cycle ambiguities. Augmentation of GPS with Iridium satellites also guarantees signal redundancy, which enables fault-detection using carrier phase Receiver Autonomous Integrity Monitoring (RAIM). Over short time periods, the temporal correlation of measurement error sources can be exploited to establish reliable error models, hence relaxing requirements on differential corrections. In this paper, a new ionospheric error model is derived to account for Iridium satellite signals crossing large sections of the sky within short periods of time. Then, a fixed-interval positioning and cycle ambiguity estimation algorithm is introduced to process Iridium and GPS code and carrier-phase observations. A residual-based carrier phase RAIM detection algorithm is described and evaluated against single-satellite step and ramp-type faults of all magnitudes and start-times. Finally, a sensitivity analysis focused on ionosphere-related system design variables (ionospheric error model parameters, code-carrier divergence, single and dual-frequency implementations) explores the potential of iGPS to fulfill some of the most stringent navigation integrity requirements with coverage at continental scales.

INTRODUCTION

Carrier phase ranging measurements from GPS and low earth orbit (LEO) Iridium telecommunication satellites are integrated in a high-integrity, precision navigation system named iGPS. iGPS opens the possibility for robust and accurate carrier phase positioning over extended geographical areas. The system's real-time, high-integrity positioning performance makes it a potential navigation solution for demanding precision applications such as autonomous terrestrial and air transportation.

Carrier phase positioning is contingent upon estimation (or resolution) of cycle ambiguities. These remain

constant as long as they are continuously tracked by the receiver. A costless yet efficient solution for their estimation is to exploit the bias observability provided by redundant satellite motion. Unfortunately, the large amount of time for GPS spacecraft to achieve significant changes in line of sight (LOS) precludes its use in real-time applications that require immediate position fixes.

In contrast, geometry variations from LEO satellites quickly become substantial. Therefore, the geometric diversity of GPS ranging sources can be greatly enhanced using additional fast moving Iridium satellites. The underlying concept of utilizing spacecraft motion to resolve cycle ambiguities is actually equivalent to the principle of Doppler positioning used in Transit, the first operational satellite radio-navigation system (starting in 1964), whose constellation was also comprised of LEO satellites. Using Transit, the position of stationary receivers could be determined with better than 70 meters of accuracy, at infrequent update intervals, based on measurements collected over 10-20min satellite passes [1]. With iGPS, the combination of Iridium LEO satellite and GPS observations makes real-time unambiguous carrier phase positioning possible without restriction on the user's motion.

In the late 1990's, Rabinowitz et al. designed a receiver capable of tracking carrier-phase measurements from GPS and from GlobalStar (another LEO telecommunication constellation) [2]. Using GlobalStar satellites' rapid geometry variations, precise cycle ambiguity resolution and positioning with respect to a nearby reference station was achieved within 5min. Numerous practical issues relative to the synchronization of GPS and GlobalStar data (without modification of the SV payload) had to be overcome to obtain experimental validation results. Rabinowitz's prior work is a compelling proof of concept for the Iridium/GPS system.

In addition, this work exploits the decisive advantage offered by iGPS in guaranteeing redundant measurements. If five or more satellites are available (always the case with Iridium-augmented of GPS), the self-consistency of the over-determined position solution is verifiable using Receiver Autonomous Integrity Monitoring (RAIM) [3]. The precision of carrier phase observations further allows for extremely tight detection thresholds while still ensuring a very low false-alarm probability.

Another dimension that plays a central part in the design of iGPS, which in this work is intended for single-frequency civilian applications, is the treatment of measurement error sources. Differential corrections can help mitigate satellite clock and orbit ephemeris errors and spatially-correlated ionospheric and tropospheric disturbances. The system, as envisioned in this preliminary analysis, aims at servicing wide-areas with minimal ground infrastructure. It must therefore rely on long-term corrections similar to the ones generated by the Wide-Area Augmentation System (WAAS) [4].

A conservative approach is adopted for the derivation of parametric measurement error models. Existing GPS measurement models used in WAAS (e.g., [5]) and in the Local Area Augmentation System (LAAS) [6] are insufficient to account for the instantaneous uncertainty at signal acquisition of iGPS observations (absolute measurement error) as well as their variations over the signal tracking duration (relative error with respect to initialization). Furthermore, the Iridium measurement error model must deal with large drifts in ranging accuracy for LEO satellite signals moving across wide sections of the atmosphere.

Measurement error models are incorporated in a fixed-interval smoothing algorithm devised for the simultaneous estimation of user position and floating carrier-phase cycle ambiguities. To protect the system against rare-event integrity threats such as user equipment and satellite failures (which may affect successive measurements during the smoothing interval) a residual-based RAIM detection algorithm is developed. It is evaluated against single-satellite step and ramp-type faults of all magnitudes and start-times.

Performance evaluations are structured around the benchmark application of aircraft precision approach. Target requirements include a 10m vertical alert limit (VAL) at touch-down, which is much tighter than what continental-scale navigation systems such as WAAS are currently able to fulfill [4]. Special emphasis is placed on integrity risk, which in this case must be lower than 10^{-9} [7].

The first section of this paper briefly presents the envisioned iGPS architecture and introduces measurement error and fault models. A refined ionospheric error model is devised and partially validated using experimental data in the second section. Estimation and detection algorithms are derived, and requirements are allocated in the third and fourth sections. Finally, in the last section of the paper, the fault-free (FF) integrity is evaluated by covariance analysis, and RAIM detection performance is quantified for a set of canonical single-satellite faults (SSF). A sensitivity analysis of the combined FF and SSF performance focuses on the impact of ionospheric disturbances and assesses the potential of iGPS to provide high-integrity and high-accuracy positioning over wide areas.

BACKGROUND

Envisioned System Architecture

Iridium's primary function is to provide telecommunication capabilities to users worldwide. Continuous global coverage is realized using 66 space vehicles (SVs), distributed among 6 planes in near-circular orbits at 86.4deg inclination, orbiting at an altitude of 780km (much lower than the 20,000km GPS orbit altitude). A 31.6deg angle separates each co-rotating orbital plane, and the remaining 22deg angle separates the two planes at the seam of the constellation, where spacecraft are counter-rotating [8]. Iridium spacecraft spend on average 10min in view of a given location on the surface of the earth, and circle the earth in a period T_{IRI} of 100min 28s [9].

As a consequence of the constellation design, the satellite density is much higher near the poles than at lower latitudes. In addition, the spacecraft trajectories generate larger North-South LOS variations relative to a ground observer than East-West. Accordingly, the horizontal carrier phase positioning performance is heterogeneous and higher iGPS positioning precision is generally achieved for the North coordinate.

A nominal 24 GPS satellite constellation is pictured in Figure 1 together with the 66 Iridium SVs. A quantitative measure of the difference between the two constellations is given by the satellites' angular velocities as perceived by an observer on earth. Let ${}^{s}\mathbf{e}_k$ be the 3×1 unit LOS vector (in a local reference frame) for satellite s at epoch k. Over a short sampling period T_P (here, T_P=30s), the angular rate between epochs $k-1$ and k is evaluated as:

$$ {}^{s}\omega_k = \cos^{-1}\left({}^{s}\mathbf{e}_{k-1}^{T} \, {}^{s}\mathbf{e}_k \right) \Big/ T_P \; . $$

The ratio of ${}^{IRI}\omega_k$ for Iridium SVs over ${}^{GPS}\omega_k$ for GPS satellites is the angular rate ratio (${}^{IRI}\omega_k$ and ${}^{GPS}\omega_k$ can be averaged over all visible Iridium and GPS satellites, respectively). It is evaluated every 30s over a 3day period to compute the average ratio. The resulting quantity equals to approximately 30 (it barely varies with location). In other words, from a user's perspective, Iridium satellites move 30 times faster than GPS. This fundamental characteristic is exploited in the estimation process for fast cycle ambiguity resolution.

In this work, the conceptual iGPS ground segment consists of a network of ground reference stations. In a first attempt to determine the overall system performance, iGPS ground stations are assumed co-located with the WAAS reference stations, whose correction accuracy has been documented over the past six years [10]. In the proposed architecture, Iridium satellite position and time synchronization information, together with WAAS-like ionospheric delay estimates and long-term GPS satellite error corrections, are derived at a master station using dual-frequency measurements collected at ground reference stations, and broadcast to the user via Iridium communication channels.

The user segment is composed of all GPS/Iridium receivers. The iGPS concept described in this work is intended for civilian users, who can collect single-frequency L-band code and carrier ranging observations. Users also have access to navigation messages for each constellation and measurement corrections. In the perspective of GPS modernization, dual-frequency GPS measurements are considered for the sensitivity analysis of longer-term future implementations. Dual-frequency Iridium signals are simulated as well.

Measurement Equation

Parametric models have been derived for measurement error sources under nominal fault-free conditions. In order to exploit changes in Iridium geometry, satellite observations are filtered over time (over an interval T_F). Measurement error models must therefore account for the instantaneous uncertainty at signal acquisition as well as variations over the signal tracking duration.

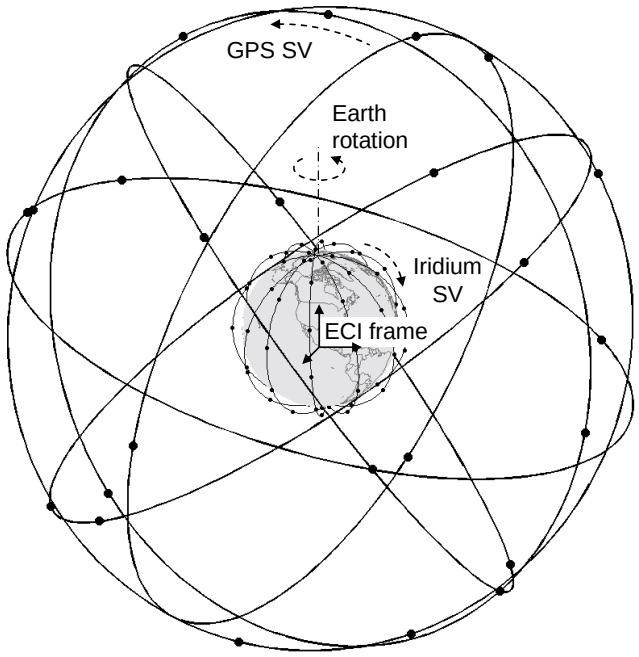

Figure 1. Joint GPS and Iridium Constellations

The complete GPS and Iridium carrier phase measurement equation for a satellite s at epoch k can be written as:

$$\begin{aligned} {}^{s}\phi_k = {}& {}^{s}r_k + \tau_k + {}^{s}N + {}^{s}ECB + \Delta t_k \cdot {}^{s}ECG \\ & - {}^{s}ob_{I,k}\left({}^{s}VIB + {}^{s}d_{IPP,k} \cdot {}^{s}VIG\right) \\ & + {}^{s}ob_{T,k}\left(ZTD + c_{T,k} \cdot \Delta n\right) \\ & + {}^{s}\varepsilon_{M-\phi,k} + {}^{s}\nu_{RN-\phi,k} \end{aligned} , \quad (1)$$

where:

${}^{s}r_k$ is the true distance between the user and satellite s,

τ_k is the user receiver clock deviation,

${}^{s}N$ is the carrier phase cycle ambiguity bias.

Parameters used to model satellite clock and orbit ephemeris errors, ionospheric and tropospheric delays, multipath and receiver noise are described in the following paragraphs.

At epoch k of the filtering interval T_F, for a satellite s that has been visible over a period Δt_k (from filter initiation to the sample time of interest), GPS and Iridium SV clock and orbit ephemeris errors are expressed as:

- an undetermined orbit ephemeris and clock bias ${}^{s}ECB$ at the time the satellite first comes in sight, which is constant over T_F; ${}^{s}ECB$ is assumed normally distributed with zero mean and variance σ^2_{ECB}; we use the notation: ${}^{s}ECB \sim \mathrm{N}(0, \sigma^2_{ECB})$.
- plus a ramp over time with an unknown but constant gradient ${}^{s}ECG_{GPS}$, accounting for linear variations from the initial value over T_F [11] (${}^{s}ECG \sim \mathrm{N}(0, \sigma^2_{ECG})$).

Nominal values for the variances σ^2_{ECB} and σ^2_{ECG} are provided in Table 1 at the end of this section (together with references justifying these values). When corrections from a WAAS-like network of reference stations are available, the $\sigma_{ECB-GPS}$ value for GPS is less than 1m. More precisely, a one-sigma root-mean-square value of 0.86m was computed using quarterly 95% range error indexes for all locations and all GPS satellites tabulated in the WAAS performance analysis reports [10] from Spring 2002 to Spring 2008 (a conservative 2m value is used in simulations). The $\sigma_{ECB-IRI}$ value of 0.1m for Iridium is realistically achievable in near-real-time using GPS receivers onboard the LEO spacecraft [12] and using Iridium's higher communication data rates (so that numerous and frequently updated orbital parameters can be exploited).

The ionospheric error model (under anomaly-free conditions in mid-latitude regions) is described in greater detail in the next section of this paper. The ionospheric delay is modeled as:

- an initial vertical ionospheric bias VIB (${}^{s}VIB \sim \mathrm{N}(0, \sigma^2_{VIB})$)
- associated to a ramp, whose constant slope over ionospheric pierce point (IPP) displacement d_{IPP} is the vertical ionospheric gradient VIG (${}^{s}VIG \sim \mathrm{N}(0, \sigma^2_{VIG})$). IPPs are defined at an altitude h_I of 350km in an earth-centered sun-fixed or ECSF frame.
- An obliquity factor ${}^{s}ob_{I,k}$, expressed as:

  $${}^{s}ob_I = \left(1 - \left[R_E \cos({}^{s}el)/(R_E + h_I)\right]^2\right)^{-1/2},$$

  where R_E is the radius of the earth, adjusts this error for the fact that the LOS pierces the ionosphere with a slant angle function of the satellite elevation angle ${}^{s}el$ (e.g., [13])

The largest part of the delay due to signal refraction in the troposphere can be removed by modeling of its dry and wet gas components [13]. The residual uncertainty is modeled as:

- a zenith tropospheric delay ZTD, which is constant over the time interval T_F ($ZTD \sim \mathrm{N}(0, \sigma^2_{ZTD})$), and
- variations relative to this initial value (caused by user motion), which are captured by a LAAS-like residual tropospheric error model expressed as a function of the local air refractivity index Δn ($\Delta n \sim \mathrm{N}(0, \sigma^2_{\Delta n})$) [6].
- The notation $c_{T,k}$ in equation 1 designates the coefficient: $10^{-6} h_0 (1 - e^{-\Delta h_k / h_0})$, where Δh_k is the difference in height that the user (e.g., aircraft) experiences from the start of the filtering interval to epoch k, and h_0 is the tropospheric scale height (a fixed value of 15km [7] is assigned).

Code and carrier phase receiver noise (${}^{s}\nu_{RN-\rho,k}$ and ${}^{s}\nu_{RN-\phi,k}$) are modeled as Gaussian white noise sequences ($\nu_{RN-\rho,k} \sim \mathrm{N}(0, \sigma^2_{RN-\rho})$ and $\nu_{RN-\phi,k} \sim \mathrm{N}(0, \sigma^2_{RN-\phi})$).

The multipath error is modeled as a first-order Gauss-Markov Process (GMP) with time constant T_M, variance $\sigma^2_{M-\phi/\rho}$ and driving noise $\nu_{M,k}$:

$${}^{s}\varepsilon_{M,k+1} = e^{-T_K/T_M} \cdot {}^{s}\varepsilon_{M,k} + \nu_{M,k}$$

with $$\nu_{M-\phi/\rho,k} \sim \mathrm{N}\left(0, \sigma^2_{M-\phi/\rho}\left(1 - e^{-2T_P/T_M}\right)\right),$$

where T_P is the sampling interval. Large azimuth-elevation variations generate fast changes in the directions

of signal reflections for Iridium. The multipath time-constant for Iridium $T_{M,IRI}$ was therefore computed by multiplying the time constant for GPS $T_{M,GPS}$ (assumed to be 60s) with the angular rate ratio between GPS and Iridium satellites (approximately 1/30 according to the previous subsection).

Equation 1 can be expressed as a function of user position $\mathbf{x}_{ENU,k}$ (for example, in a local East-North-Up frame), LOS vector ${}^{s}\mathbf{e}_k$ and clock deviation τ_k. Typically in GPS navigation, the measurement ${}^{s}\phi_k$ is linearized about an approximated user position vector (which is iteratively refined using a Newton-Raphson approach [13]). The linearized carrier phase observation is defined as:

$$\begin{aligned} {}^{s}\phi_{L,k} = {}& {}^{s}\mathbf{g}_k^T\mathbf{u}_k + {}^{s}N + {}^{s}ECB + \Delta t_k \cdot {}^{s}ECG \\ & + {}^{s}ob_{T,k}\left(ZTD + c_{T,k}\cdot\Delta n\right) \\ & - {}^{s}ob_{I,k}\left({}^{s}VIB + {}^{s}d_{IPP,k}\cdot{}^{s}VIG\right) \\ & + {}^{s}\varepsilon_{M-\phi,k} + {}^{s}\nu_{RN-\phi,k} \end{aligned} \quad , \qquad (2)$$

where ${}^{s}\mathbf{g}_k^T = [{}^{s}\mathbf{e}_k^T \quad 1]$ and $\mathbf{u}_k = [\mathbf{x}_{ENU,k}^T \quad \tau_k]^T$. The equation for the linearized code phase measurement ${}^{s}\rho_{L,k}$ is identical except for the absence of cycle ambiguity bias ${}^{s}N$, a positive sign on the ionospheric error, and the code receiver noise ${}^{s}\nu_{RN-\rho,k}$ and multipath ${}^{s}\varepsilon_{M-\rho,k}$ which replace ${}^{s}\nu_{RN-\phi,k}$ and ${}^{s}\varepsilon_{M-\phi,k}$, respectively.

In summary, error parameter values for the nominal configuration (listed in Table 1) were selected to describe a system architecture implementable in the short term, for single-frequency GPS/Iridium users. The nominal configuration assumes that users are provided with GPS ephemeris and clock data, precise Iridium satellite orbit and clock information, as well as WAAS-like GPS satellite clock and orbit ephemeris corrections and ionospheric corrections. An estimated 10min upper-limit $T_{F,MAX}$ is fixed on the validity of the error models.

Finally, the assertion that error models are conservative is only true if the Gaussian models over-bound the cumulative distribution functions of each error sources' nominal ranging errors [14]. The next phase of this research consists in establishing probability distributions for the error parameters, and in verifying the fidelity of the dynamic models to experimental data. Alternatively, parameter values in Table 1 may be considered as requirements that ground corrections should meet in order to achieve the desired system performance.

Table 1. Summary of Error Parameter Values

Parameter	Nominal Value	Ref.	Parameter	Nominal Value	Ref.
$\sigma_{ECB-GPS}$	2m	[10]	σ_{VIG} *	4mm/km	[16]
$\sigma_{ECG-GPS}$	$4.72\cdot10^{-4}$m/s	[15]	$\sigma_{RN-\rho}$ **	0.3m	
$\sigma_{ECB-IRI}$	0.1m	[12]	$\sigma_{RN-\phi}$ **	0.003m	
$\sigma_{ECG-IRI}$	$4.57\cdot10^{-4}$m/s	[15]	$\sigma_{M-\rho}$ **	1m	
σ_{ZTD}	0.12m	[4]	$\sigma_{M-\phi}$ **	0.01m	
$\sigma_{\Delta n}$	30	[7]	$T_{M,GPS}$	1min	
σ_{VIB} *	1.5m	[10]	$T_{M,IRI}$	2s	

* for dual-frequency: VIG and VIB terms are eliminated

** for dual-frequency (at f_1 and f_2), these terms are multiplied by $([f_1^2/(f_1^2-f_2^2)]^2+[f_2^2/(f_1^2-f_2^2)]^2)^{1/2}$

Single-Satellite Fault Models

Measurement errors, whose magnitude, distribution and dynamics are not accounted for in the above nominal models, are referred to as faults. They correspond to rare events such as equipment and satellite failures or unusual atmospheric conditions. A set of canonical single-satellite threat models is established. Simulated impulse, step and ramp-type fault vectors (noted $\mathbf{f}$) of arbitrary magnitude (the worst case magnitude is determined as part of the RAIM detection method described below), and spanning the entire range of possible starting times (at regular intervals T_B of 5s or less over the filtering period T_F), are constructed for all measurements collected during the filtering duration T_F. Faults are applied to code and carrier phase measurements individually as well as simultaneously, one SV at a time. As a result, the number of simulated threat models exceeds 7000 for a ten-minute filtering interval. Fault models will later be deliberately injected into simulated measurements to evaluate the performance of the fault-detection algorithm.

At this stage of this research, simulated faults are limited to satellite failures because they are the only types of faults for which the failure rate FR is reliably known. Reference [17] specifies that the satellite service failure frequency should not exceed three per year for the entire GPS constellation. In fact, the GPS ground segment monitors the satellite's health to minimize the probability of faults. Finally, steps and ramps account for a large part of the satellite faults, including signal deformation, code-carrier divergence, excessive clock deviations and erroneous ephemeris parameters.

REFINED IONOSPHERIC ERROR MODEL

An upper limit (noted $d_{IPP,MAX}$) is fixed on IPP displacements to ensure the validity of the ionospheric error model. This $d_{IPP,MAX}$ limit is occasionally exceeded by fast moving Iridium satellites, which cross large sections of the ionosphere within less than 10min. In this section, a refined ionospheric error model is presented and partially validated using experimental data from Continuously Operating Reference Stations (CORS) for high-elevation satellite signals.

Piecewise Linear Model of Vertical Ionospheric Delay

The residual ionospheric error model implemented in this work (under anomaly-free conditions in mid-latitude regions) hinges on three major assumptions.

- The ionosphere is assumed constant over short periods of times in an earth-centered sun-fixed (ECSF) frame (whose x-axis is pointing toward the sun and whose z-axis is the earth's axis of rotation) [18].
- A spherical thin shell approximation is adopted to localize the effect of the ionosphere at the altitude h_I where the peak electron density occurs (we assume that h_I=350km). An ionospheric pierce point (IPP) is defined as the intersection between the satellite-user LOS and the thin shell. A one-dimensional model is employed assuming that GPS and Iridium IPP traces are straight paths along the great circle over short time periods.
- The vertical ionospheric delay varies linearly with IPP separation distances (actually 'great circle distances' or GCD) of up to 2000km [5]. The distribution of the corresponding slope can be bounded by a Gaussian model [19].

As mentioned in the "Background" section, the equivalent slant ionospheric delay (for code) or advance (for carrier) is given by:

$$ {}^s\varepsilon_{I,k} = {}^s ob_{I,k} \cdot \left({}^s VIB + d_{IPP,k} \cdot {}^s VIG \right). \qquad (3) $$

Iridium SVs move across much wider sections of the ionosphere than GPS satellites. The average ratio of Iridium over GPS IPP displacements was computed at mid-latitudes for SV geometries simulated over a three day period at 30s intervals: the ratio is constant for displacements over 1-10min and varies with latitude between 10 (at the Miami location) and 12 (Chicago). Also, within 10min, the average Iridium IPP velocity in an ECSF frame, computed over a three-day period, is 245km/min (it is constant over CONUS), and the average IPP velocity for GPS varies between 21km/min (Chicago) and 25km/min (Miami).

The maximum GCD traveled by an Iridium IPP when occasionally crossing the sky with near-zero azimuth is reached in approximately 10min. Using an expression of the earth central angle (the angle between the satellite, the center of the earth and the user) [8] and for an elevation mask angle el_{min} of 5deg, the maximum IPP displacement can be expressed as:

$$ 2\left(R_E + h_I\right)\left(\cos^{-1}\left(\frac{R_E \cdot \cos\left(el_{min}\right)}{R_E + h_I} \right) - el_{min} \right). $$

This number amounts to 3300km, which is larger than the suggested $d_{IPP,MAX}$ limit of 2000km. To circumvent this problem, equation 3 is applied piecewise over less-than-2000km-long segments of the satellite pass. In practice, a satellite s whose d_{IPP} exceeds the limit between epochs k and $k+1$ is attributed a new gradient ${}^sVIG_N$ (with ${}^sVIG_N \sim \mathrm{N}(0, \sigma^2_{VIG})$), so that the ionospheric error at epoch $k+j$ posterior to k becomes:

$$ {}^s\varepsilon_{I,k+j} = {}^s ob_{I,k+j} \cdot \left({}^s VIB + d_{IPP,0:k} \cdot {}^s VIG + d_{IPP,k+1:k+j} \cdot {}^s VIG_N \right) $$

where $d_{IPP,i:j}$ is the IPP displacement between epochs i and j.

This piecewise linear model of the vertical ionospheric delay is described in Appendix 1 for implementations in a Kalman filter and in a weighted least-squares batch algorithm. The $d_{IPP,MAX}$ limit can be set as small as desired by introducing multiple new states ${}^sVIG_N$ (the extreme case being to add one new state per sample time). The selection of $d_{IPP,MAX}$ is driven by the following tradeoff: the smaller the $d_{IPP,MAX}$ parameter, the better the fidelity of the model to experimental data (as demonstrated in the next subsection), but also the lower the iGPS positioning and fault detection performance (which is quantified in the section entitled "Performance Evaluation").

Preliminary Ionospheric Error Model Validation for High-Elevation Satellites

The fidelity of the ionospheric error model (equation 3) to experimental data is evaluated for segments of the linear fit ranging from 200km to 1700km (i.e., for $d_{IPP,MAX}$ ranging from 200km to 1700km).

The ionospheric delay is proportional to the total electron content in the path of the signal and to the inverse square of the carrier frequency. This frequency-dependence can be exploited with dual-frequency signals to measure ionospheric disturbances.

Dual-frequency GPS carrier-phase observations (noted ϕ_{L1} and ϕ_{L2}, in units of meters, at frequencies

f_{L1}=1575MHz and f_{L2}=1228MHz) from CORS are processed to evaluate the ionospheric delay on L1 signals (at f_{L1} frequency). A biased and noisy measure of the ionospheric delay is obtained by differencing L1 and L2 observations (many terms in equation 2 cancel, see for example [13]):

$$z_{I,k} = \frac{f_{L2}^2}{f_{L1}^2 - f_{L2}^2}(\phi_{L1,k} - \phi_{L2,k}),$$

which, using the model of equation 3, can be written as:

$$z_{I,k} = ob_k\left(VIB + d_{IPP,k}\cdot VIG\right) + b_I + v_{I,k}, \qquad (4)$$

where b_I is a constant bias that includes the differenced L1-L2 cycle ambiguity and inter-frequency biases. The measurement noise $v_{I,k}$ is a time-correlated random sequence whose standard deviation should not exceed 2.3cm (a conservative value computed using the values of Table 1); $v_{I,k}$ is expressed as (assuming that the effect of multipath and receiver noise are the same on L1 and L2):

$$v_{I,k} = \sqrt{2}\,\frac{f_{L2}^2}{f_{L1}^2 - f_{L2}^2}\left(\varepsilon_{M-\phi,k} + v_{RN-\phi,k}\right).$$

In this work, observations $z_{I,k}$ collected over a finite fit interval (from epoch 0 to k_{MAX}, corresponding to a displacement $d_{IPP,MAX}$) are stacked in a measurement vector in order to simultaneously estimate the constant parameters VIB, VIG and b_I:

$$\begin{bmatrix} z_{I,0} \\ \vdots \\ z_{I,k_{MAX}} \end{bmatrix} = \begin{bmatrix} ob_{I,0} & ob_{I,0}\cdot d_{IPP,0} & 1 \\ \vdots & \vdots & \vdots \\ ob_{I,k_{MAX}} & ob_{I,k_{MAX}}\cdot d_{IPP,k_{MAX}} & 1 \end{bmatrix} \begin{bmatrix} VIB \\ VIG \\ b \end{bmatrix} + \begin{bmatrix} v_0 \\ \vdots \\ v_{k_{MAX}} \end{bmatrix}$$

Unlike other data processing techniques that are limited by the change in satellite geometry (e.g., assuming constant $ob_{I,k}$ over short periods [16]), this method exploits the observability provided by the relative change in coefficients $ob_{I,k}$, $ob_{I,k}\cdot d_{IPP,k}$ and 1.

The fidelity of the measurement model in equation 4 is quantified by computing residual errors after detrending the data (i.e., after removing the estimated main trend $ob_k(VIB + d_{IPP,k}\cdot VIG) + b_I$ from the actual data). Residual errors are made of measurement noise $v_{I,k}$ and process noise (i.e., errors caused by mis-modeling).

A set of GPS data collected at the Holland, MI CORS site during the months of January to August 2007 is considered. This time period comprises 91 days of quiet ionospheric activity (classified in terms of A-indexes [20]), 126 unsettled days and 16 active days. In this preliminary analysis, an elevation mask of 50deg is implemented. The set of data is processed for fit intervals of varying lengths, corresponding to $d_{IPP,MAX}$ values ranging from 200km to 1700km in increments of about 50km.

Figure 2 presents the distribution of the residual error versus $d_{IPP,MAX}$. Within each bin of $d_{IPP,MAX}$, colors designate the percentage of occurrences of a given residual error value. The total number of residual error data points in each bin is approximately 200,000. White lines indicate the 1-sigma envelope. A large majority of residual errors remain lower than 5cm, for all $d_{IPP,MAX}$. Since the same set of data is processed in each vertical bin, the measurement noise is expected to be the same for all $d_{IPP,MAX}$ values. Therefore, the widening of the residual's distribution as $d_{IPP,MAX}$ increases is attributed to modeling errors. For our current purposes, a nominal $d_{IPP,MAX}$-value of 750km is selected, for which modeling errors are deemed negligible with respect to the expected measurement noise level.

Further experimental data processing will determine whether the model is still valid at low elevation, and during days of higher ionospheric activity, at the peak of the solar cycle.

IGPS ALGORITHMS

Models of the dynamics and probability distributions for the measurement error sources described above are a crucial input to the estimation and detection algorithms.

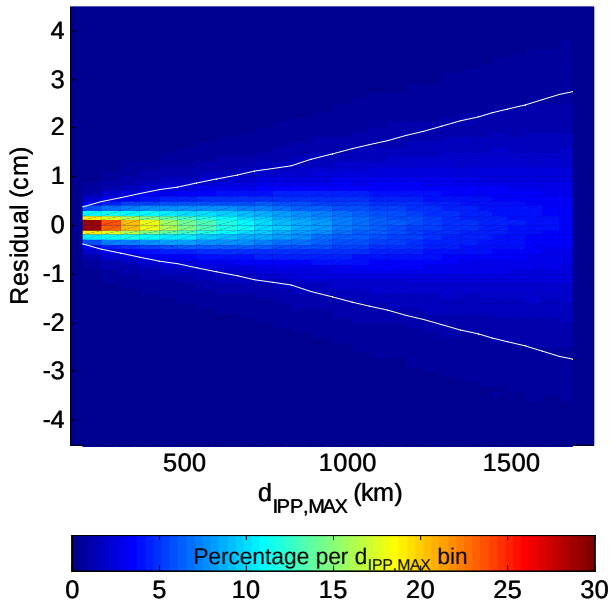

Figure 2. Fidelity of the Model to High-Elevation Satellite Data

iGPS Estimation Algorithm

A fixed-interval smoothing algorithm has been devised for the simultaneous estimation of user position and floating carrier phase cycle ambiguities. It is compatible with real-time implementations provided that sufficient memory is allocated to the storage of a finite number of past measurements and LOS coefficients. Current-time optimal state estimates are obtained from iteratively feeding the stored finite sequence of observations into a Kalman filter (KF).

In anticipation of the RAIM-type residual-based fault detection introduced in the following subsection, a fixed-interval smoothing (instead of filtering) process is used. A batch measurement processing method is presented below for clarity in exposition. Batch processing produces results identical to the KF for the current time, as well as optimal estimates for past epochs that are later used for residual generation.

Consider first the vector of carrier phase observations for a satellite s in view between epochs k_O and k_F (k_O and k_F are the first and last epochs of the smoothing interval if satellite s is visible during the entire interval T_F):

$$ {}^{s}\boldsymbol{\varphi} = \left[\begin{array}{ccc} {}^{s}\phi_{k_O} & \cdots & {}^{s}\phi_{k_F} \end{array} \right]^T . $$

Carrier phase observations for all n_S Iridium and GPS satellites are then stacked together:

$$ \boldsymbol{\varphi} = \left[\begin{array}{ccc} {}^{1}\boldsymbol{\varphi}^T & \cdots & {}^{n_S}\boldsymbol{\varphi}^T \end{array} \right]^T . $$

A state space representation of vector $\boldsymbol{\varphi}$ is realized based on equation 2. Error parameters and their dynamic models are incorporated by state augmentation. The carrier phase measurement equation is written in the form:

$$ \boldsymbol{\varphi} = \mathbf{H}_{\boldsymbol{\varphi}} \mathbf{x} + \mathbf{v}_{\boldsymbol{\varphi}} , \qquad (5) $$

where $\mathbf{v}_{\boldsymbol{\varphi}}$ designates the carrier phase measurement noise vector and the observation matrix $\mathbf{H}_{\boldsymbol{\varphi}}$ is defined in Appendix 2. The state vector $\mathbf{x}$ is equal to:

$$ \left[\begin{array}{ccccccccc} \mathbf{u}_{k_O}^T & \cdots & \mathbf{u}_{k_F}^T & \mathbf{N}^T & \mathbf{ECB}^T & \mathbf{ECG}^T & ZTD & \Delta n & \mathbf{VIB}^T \quad \mathbf{VIG}^T \end{array} \right]^T $$

Bold face characters for parameters other than $\mathbf{u}_k$ designate vectors of states for all satellites, such as for example:

$$ \mathbf{N} = \left[\begin{array}{ccc} {}^{1}N & \cdots & {}^{n_S}N \end{array} \right]^T . $$

The dynamics of the user position and clock deviation vector $\mathbf{u}_k$ are unknown. Different states are therefore allocated to the vector $\mathbf{u}_k$ at each time step, as opposed to the other parameters that are modeled as constants over interval T_F.

A measurement equation similar to equation 5 is established for the code-phase observation vector $\boldsymbol{\rho}$ (see Appendix 2 for details).

The complete sequence of code and carrier phase signals for all satellites over the smoothing interval are included into a batch measurement vector:

$$ \mathbf{z} = \left[\begin{array}{cc} \boldsymbol{\varphi}^T & \boldsymbol{\rho}^T \end{array} \right]^T , $$

and

$$ \mathbf{z} = \mathbf{H}\mathbf{x} + \mathbf{v} . \qquad (6) $$

The measurement noise vector $\mathbf{v}$ (with covariance $\mathbf{V}$) is utilized to introduce the time-correlated noise due to multipath as well as receiver noise (Appendix 2).

Prior knowledge on the error parameters is expressed in terms of bounding values on their probability distributions. The a-priori information matrix $\mathbf{V}_P^{-1}$ on the error states $\mathbf{ECB}$, $\mathbf{ECG}$, ZTD, Δn, $\mathbf{VIB}$ and $\mathbf{VIG}$ is diagonal, with diagonal vector:

$$ \left[\begin{array}{ccccccc} \mathbf{1}_{1\times n_S}\sigma_{ECB}^{-2} & \mathbf{1}_{1\times n_S}\sigma_{ECG}^{-2} & \sigma_{ZTD}^{-2} & \sigma_{\Delta n}^{-2} & \mathbf{1}_{1\times n_S}\sigma_{VIB}^{-2} & \mathbf{1}_{1\times n_S}\sigma_{VIG}^{-2} \end{array} \right] $$

where $\mathbf{1}_{1\times n}$ is a $1\times n$ column-vector of ones.

The weighted least-squares state estimate covariance, with prior knowledge on the error states, is expressed as:

$$ \mathbf{P}_{\mathbf{x}} = \left(\left[\begin{array}{cc} \mathbf{0} & \mathbf{0} \\ \mathbf{0} & \mathbf{V}_P^{-1} \end{array} \right] + \mathbf{H}^T\mathbf{V}^{-1}\mathbf{H} \right)^{-1} . $$

The weighted least squares state estimate $\hat{\mathbf{x}}$ is obtained using the equation (e.g., [21]):

$$ \hat{\mathbf{x}} = \mathbf{S}\ \mathbf{z} , $$

where $\mathbf{S}$ is the weighted pseudo-inverse of $\mathbf{H}$:

$$ \mathbf{S} = \mathbf{P}_{\mathbf{x}}\mathbf{H}^T\mathbf{V}^{-1} $$

Finally, the diagonal element of $\mathbf{P}_{\mathbf{x}}$ corresponding to the current-time vertical position covariance (noted σ_U^2) is used later to establish an availability criterion under fault-free conditions. The focus is on the Up-coordinate, both because of the tighter requirements in this direction and because of the generally higher vertical dilution of precision (VDOP) as compared to horizontal coordinates.

Batch Residual RAIM Detection Algorithm

State estimation is based on a history of observations, all of which are vulnerable to satellite faults. To protect the system against abnormal events, a RAIM-type process is implemented, using the least-squares residuals of the batch measurement equation 6.

The least-squares residual RAIM methodology [3] gives a statistical description of the impact of a measurement fault vector $\mathbf{f}$ (of same dimensions as $\mathbf{z}$), whose non-zero elements introduce deviations from normal FF conditions. Equation 6 becomes:

$$\mathbf{z} = \mathbf{H}\mathbf{x} + \mathbf{v} + \mathbf{f} .$$

The RAIM procedure is articulated around two dimensions.

First, the fault vector $\mathbf{f}$ impacts the state estimate error. Let $\mathbf{s}_{U,k_F}^T$ be the row of $\mathbf{S}$ corresponding to the vertical position at the last (i.e., current-time) epoch k_F of the smoothing interval. The system is said to produce hazardous information if the corresponding positioning error δx_U ($\delta x_U \sim \mathrm{N}(\mathbf{s}_{U,k_F}^T \mathbf{f}, \sigma_U^2)$) exceeds a vertical alert limit *VAL* :

$$\left|\delta x_U\right| > VAL .$$

Second, the fault $\mathbf{f}$ may be detected using the residual vector $\mathbf{r}$, which can be expressed as: $\mathbf{r} = (\mathbf{I} - \mathbf{HS})(\mathbf{v} + \mathbf{f})$. The norm of $\mathbf{r}$ weighted by the measurement noise information matrix $\mathbf{V}^{-1}$ is used as a test statistic: $\|\mathbf{r}\|_W^2 = \mathbf{r}^T \mathbf{V}^{-1} \mathbf{r}$. A detection threshold R_C is set in compliance with a continuity requirement P_C to limit the probability of false alarms under fault free conditions [22]. As a result, a measurement failure is undetected if:

$$\|\mathbf{r}\|_W < R_C .$$

The probability of missed detection (MD) P_{MD} is defined as a joint probability:

$$P_{MD} = P\left(\left|\delta x_U\right| > VAL \ , \ \|\mathbf{r}\|_W < R_C \right).$$

The probability P_{MD} is used in the next section to determine whether the integrity requirement is met under faulty conditions.

FRAMEWORK FOR THE ANALYSIS

Integrity Requirement Allocation

For iGPS to be validated as a navigation solution for applications such as autonomous transportation, it must demonstrate the ability to fulfill an overall integrity requirement. In this work, the overall integrity risk requirement, or probability of hazardous misleading information (HMI), is noted P_{HMI}. It represents the total integrity budget that must be allocated to individual system components in order to ensure safe user navigation under fault-free (FF), single-satellite fault (SSF) and all other conditions.

In this work, an integrity risk P_ε is allocated to cases of multiple SV faults occurring during the same time interval T_F. Multiple simultaneous faults are considered independent events and hence have a low probability of occurrence. The prior probability p_P for an individual satellite fault, with failure rate FR, occurring during the exposure period T_F, is defined as: $p_P = FR \cdot T_F$. Therefore, the value allocated to P_ε can be selected larger than the probability of two or more faults occurring during T_F, so that:

$$P_\varepsilon \geq 1 - \sum_{i=0}^{1} C_i^{n_S} \, p_P^i \left(1 - p_P\right)^{n_S - i} ,$$

where $C_k^{n_S}$ is the binomial coefficient. For a 10min exposure period T_F and using measurements from seven different SVs, the probability P_ε is approximately 10^{-10}.

An integrity budget of $\alpha(P_{HMI} - P_\varepsilon)$ is allocated to normal FF conditions, and the remaining fraction $(1-\alpha)(P_{HMI} - P_\varepsilon)$ is attributed to SSF. The coefficient α ranges between 0 and 1; a value of 10^{-3} is selected for the nominal configuration.

Requirements and Availability Criteria for a Benchmark Application of Aircraft Precision Approach

For the benchmark application of aircraft precision approach, the integrity risk requirement P_{HMI} specifies that when the pilot has near-zero visibility to the runway, no more than one event leading to hazardous misleading navigation information is allowed in a billion approaches ($P_{HMI} = 10^{-9}$) [7].

Under normal conditions, the vertical protection level *VPL* is defined as a function of the standard deviation of the vertical position coordinate σ_U :

$$VPL = \kappa_{FF} \cdot \sigma_U ,$$

where the probability multiplier κ_{FF} is the value for which the normal cumulative distribution function equals $1 - \alpha(P_{HMI} - P_\varepsilon)/2$. In accordance with civilian aviation standards, which specify a vertical alert limit *VAL* of 10m from 200 feet of altitude to TD, an approach is deemed available under FF conditions if and only if:

$$VPL < VAL . \qquad (7)$$

Rare-event faults such as equipment and satellite failures (whose rate FR is approximately $4 \cdot 10^{-9}$/s) become significant threats when aiming at ensuring an integrity risk $(1-\alpha)(P_{HMI} - P_\varepsilon)$ on the order of 10^{-9}. The RAIM methodology is implemented to evaluate the impact of such faults. The detection threshold is set in compliance with a continuity requirement P_C of $2 \cdot 10^{-6}$ to limit the probability of false alarms [7]. For each simulated fault type (bias, ramp and impulse), the RAIM algorithm determines the fault causing the highest probability of missed detection P_{MD} over all satellites (identified with the subscript *sv*), all fault magnitudes (subscript *mag*)

and all fault breakpoints (i.e., starting times, with a subscript bkp). In order to speed up the screening of simulated faults, two SSF-availability criteria are established. The first conservative criterion specifies that:

$$\max_{sv,mag,bkp}\left(P_{MD}\right) FR\cdot T_F < (1-\alpha)\left(P_{HMI}-P_{\varepsilon}\right). \quad (8)$$

The criterion of equation 8 is conservative because it assumes that the probability P_{MD} maintains its highest level for faults staring at different times during the exposure period T_F. In fact, the maximum P_{MD} varies considerably for fault breakpoints at varying times during T_F. Instead of considering the worst case over T_F, the probabilities $P_{MD,bkpt}$ can be summed for all faults starting at regular time intervals T_B (T_B=5s):

$$\sum_{bkp}\max_{sv,mag}\left(P_{MD,bkp}\right) FR\cdot T_B < (1-\alpha)\left(P_{HMI}-P_{\varepsilon}\right). \quad (9)$$

The summation on the left-hand-side term of equation 9 is time-consuming to compute, but it only needs to be performed if the conservative criterion of equation 8 is not met. Finally, if equation 9 is not satisfied, the approach or geometry is deemed SSF-unavailable.

Equations 7 and 9 are the expressions of FF and SSF binary criteria that either validate or nullify availability for an approach. During an approach, the airplane is assumed to follow a straight-in trajectory at a constant speed of 70m/s with a 3deg glide-slope angle towards the runway until touchdown (TD) where requirements apply. In the following section, aircraft approaches starting at regular intervals are simulated for T_F-long sequences of satellite-user geometries, over a period T_{AV} defined below. Ultimately, the percentage of available approaches is the measure of iGPS FF and SSF performance.

PERFORMANCE EVALUATION

In this section, the performance sensitivity to ionospheric error parameters is quantified, the importance of code-carrier divergence is evaluated, and the potential of dual-frequency implementations is investigated for multiple locations over the United States and Europe. Results are presented in terms of 'combined availability', which is only granted for an approach if both FF and SSF criteria are satisfied. The SSF criterion is the driving factor for loss of availability.

Nominal System Configuration

iGPS performance is first established for a nominal system configuration (i.e., for a near-term future iGPS architecture presented in the "Background" section). The Miami location is selected, because the Iridium satellite geometry at this southern latitude is one of the poorest for the contiguous United States (CONUS).

Table 2. Summary of Nominal Simulation Parameters

Parameter	Description	Nominal
T_F	Filtering period	8min
T_P	Sampling interval (different from positioning interval)	30s
T_B	Interval between simulated fault breakpoints	5s
T_{AV}	Availability simulation period	3 days
	Interval between simulated approaches	30s
Location	Near-worst case (25.5deg North, -81.1deg East)	Miami
Signals	Single-frequency (SF) or dual-frequency (DF)	SF
	GPS constellation	24 SVs
	Iridium constellation	66 SVs

A summary of nominal simulation parameters is given in Table 2. A smoothing period T_F of 8 minutes (such that $T_F < T_{F,MAX}$) is chosen to investigate availability performance variations. The sample time T_P (T_P=30s) and the time between fault breakpoints T_B (T_B=5s) were selected to decrease the computational load while not influencing availability results.

Of particular importance when combining measurements from multiple constellations is the duration T_{AV} over which availability simulations are carried out. The period T_{AV} should enable sampling of a complete set of satellite geometries. It takes 1,507 sidereal days (more than 4 years) for the geometry between the earth, GPS and Iridium satellites to completely repeat itself. Simulating the algorithms over 1,507 days is computationally too intensive. Fortunately, an approximated duration representative of a large number of geometries can be utilized for the joint constellation. In fact, Iridium satellites circle the earth exactly 43 times in three solar days and four seconds. Concurrently, it is important that the interval between simulated approaches be selected short enough to not influence the quantitative availability results. Approaches are therefore simulated every 30s over a period T_{AV} of three days.

Sensitivity to Ionospheric Error Model Parameters

The performance sensitivity to VIB and VIG is investigated for realistic ranges of values in Figure 3. More precisely, the combined FF-SSF availability at the

Miami location is plotted for each parameter's nominal standard deviation σ_{NOM} (listed in Table 1 – e.g. for VIB, σ_{NOM} is σ_{VIB} in that table) scaled by $i/5$, where i is an integer ranging from 1 to 9. As expected, values lower than σ_{NOM} produce better results than the nominal case, and conversely availability decreases for higher values.

Availability performance is very sensitive to the standard deviation of the vertical ionospheric bias σ_{VIB}. The VIB parameter has a more significant impact than the gradient VIG. The accumulated error for the gradient term $ob_I d_{IPP} VIG$ over the short filtering interval is not nearly as large as the bias-term $ob_I VIB$.

In the absence of ionospheric corrections, σ_{VIB} may easily exceed 3m (which is larger than $9 \cdot \sigma_{NOM} / 5$ on the x-axis) causing availability to sink. This is evidence that single-frequency iGPS without corrections from a sizeable network of ground stations is not sufficient to enable applications that require high accuracy and integrity. Still, assuming a σ_{VIB} of 5m, analysis has shown that the system produces 99% combined availability at latitudes higher than 45deg. (The latitude of Miami is 25.5deg.) Performance sensitivity to location is investigated below.

In addition, FF and SSF availability performance is evaluated in Figure 4 for values of $d_{IPP,MAX}$ ranging from 100km to 2000km. As the model's fit interval ($d_{IPP,MAX}$) decreases and the number of additional ${}^{s}VIG_N$ states increases (each one introducing an initial uncertainty σ_{VIG}), availability decreases. A sharp drop in performance occurs for $d_{IPP,MAX}$ values lower than 600km. This result was taken into account when selecting the nominal $d_{IPP,MAX}$ value of 750km.

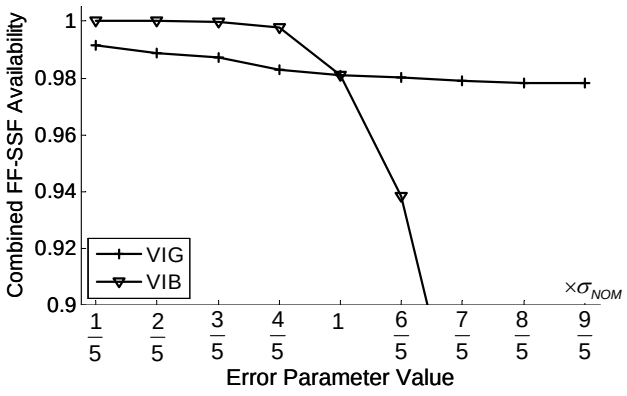

Figure 3. Performance Sensitivity to VIB and VIG

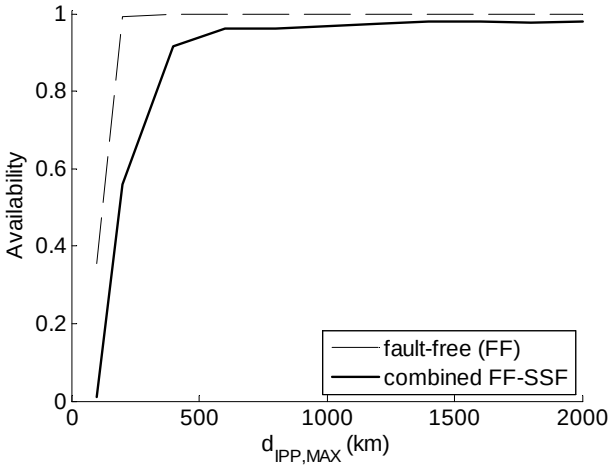

Figure 4. Performance Sensitivity to $d_{IPP,MAX}$

Influence of Code Phase Measurements

In this subsection, iGPS performance is first evaluated for comparison with filtering only WAAS corrected GPS code and carrier measurements (i.e., without Iridium). In the upper graph of Figure 5, VPLs are computed for the nominal configuration at the Miami location, over a 15-hour period (extracted out of the total 3-day T_{AV} period). In contrast with the iGPS implementation (thin solid line), filtering WAAS/GPS measurements over the period T_F brings little positioning improvement, so that VPL variations for WAAS/GPS (dashed line) are nearly proportional to VDOP.

Nominal iGPS performance is mostly influenced by Iridium satellite geometry. For example, low VPLs are achieved at the seam of the constellation where satellite density is higher (on the x-axis, during intervals 2-3hrs and 14-15hrs). Also, local VPL minima are generated at regular 2hour intervals where the user location crosses an orbital plane (user location moves in ECI because of earth rotation). In these cases, Iridium satellites moving overhead the user location generate large variations in vertical LOS coefficients, hence providing greater observability on cycle ambiguities.

Information provided by code phase observations plays a considerable part in the estimation process, especially in cases of poor Iridium satellite geometry. To illustrate this statement, VPLs are also computed in Figure 5 without using Iridium code measurements (upper chart) and without GPS code pseudoranges (lower chart).

The VPL saw tooth pattern in the upper chart (thick solid line: without Iridium code) is driven by the ionospheric error's influence on Iridium signals, which varies with Iridium satellite elevation. As described in the error

model, coefficients for the ionospheric error states (*VIB* and *VIG*) are negative for carrier observations and positive for code. This code-carrier divergence provides observability on *VIB* and *VIG*. In addition, the obliquity factor ${}^{s}ob_{I,k}$ increases as the elevation angle decreases. Without Iridium code data, code-carrier divergence can no longer be exploited, and the ionosphere's impact on the vertical position estimate is accentuated for low-elevation SV signals. Therefore, low VPLs are achieved when the user location is close to an Iridium orbital plane (high-elevation SVs coinciding with local VPL minima). VPLs increase gradually as the user location moves away from the orbital plane (due to earth rotation) until a local maximum is reached right in between two planes (low-elevation SVs). The comparison with the nominal case (thin solid curve) reveals the contribution of the code-carrier divergence for Iridium measurements.

In the lower graph of Figure 5, the absence of GPS code measurements results in peaks of VPL occurring on both sides of the local minima. These intervals have been identified as cases of poor Iridium satellite geometries, where biases in the East and Up position coordinates are unobservable (because LOS coefficient variations over T_F are nearly identical in these two directions). Therefore, without the coarse GPS code-based user position estimate, rapid cycle ambiguity estimation becomes extremely challenging. Even though Iridium carrier phase signals carry the most weight in the estimation, it is apparent that code and carrier phase measurements from both constellations are instrumental in achieving high-integrity FF performance.

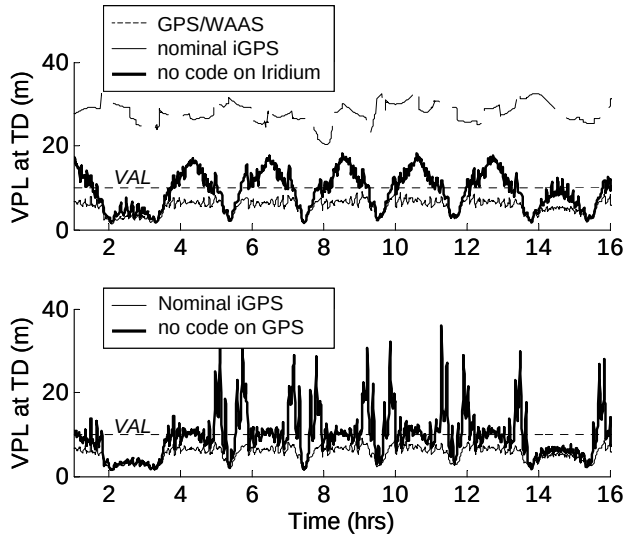

Figure 5. Influence of Code Phase Measurements
Performance Sensitivity to Location

Combined FF and SSF availability (for the nominal configuration) is presented for a 5deg×5deg and a 4deg×4deg latitude-longitude grid of locations respectively over CONUS and over Europe in Figure 6. As expected, results improve at higher latitudes, as the density of Iridium satellites increases.

If user receivers can track ranging measurements at multiple frequencies (e.g., GPS L1 and L5 signals will become available for civilian users within the next decade), ionospheric-free observations can be implemented. In this case, the iGPS performance increases substantially as illustrated in Figure 7: for example, for the grid point location near Miami, availability increases from 98.28% for the nominal single-frequency configuration to 99.14% using dual-frequency GPS signals.

Finally, if both GPS and Iridium were to provide dual-frequency measurements (Figure 8), iGPS performance would no longer be impacted by ionospheric disturbances, and availability would exceed 99.9% for all locations.

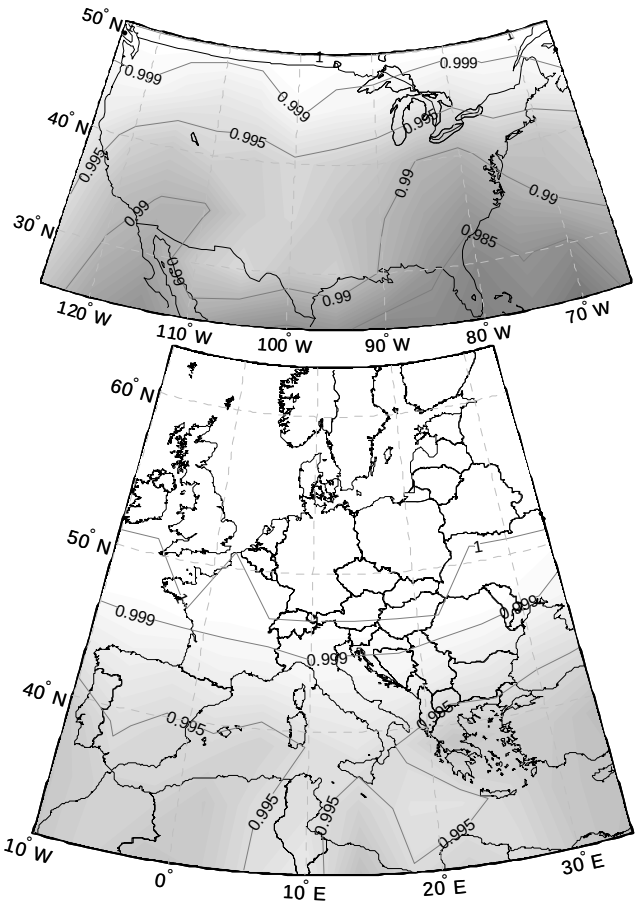

Figure 6. Nominal Availability Maps (Single-Frequency GPS and Iridium)

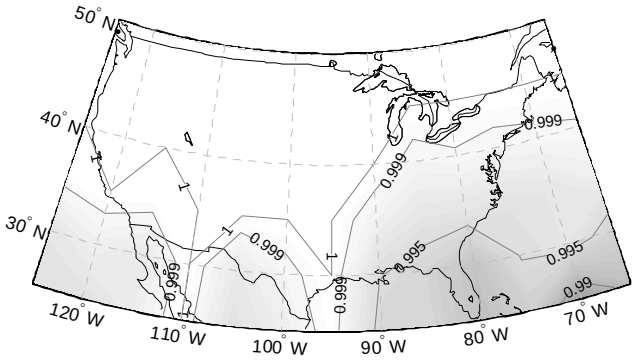

Figure 7. Availability Map For Dual-Frequency GPS (Single-Frequency Iridium)

CONCLUSION

This paper investigates the potential for Iridium-augmented GPS to enable rapid, robust and accurate navigation at continental scales. The treatment of ionospheric errors (for single-frequency civilian users) is particularly challenging. An initial ionospheric error model has been derived and partially validated for high elevation GPS satellite signals. Further experimental data analysis is necessary to quantify the model's fidelity to actual data, and to identify and characterize ionospheric anomalies.

Early performance analysis results over CONUS and Europe demonstrate that single-frequency iGPS can come close to fulfilling some of the most stringent standards currently in effect for civilian aircraft navigation. Future evolutions including dual-frequency architectures yield an even more decisive impact for Iridium-augmented GPS, as they may relax the requirements on ground infrastructure while extending the availability of high-integrity carrier-phase positioning from wide areas to the entire globe.

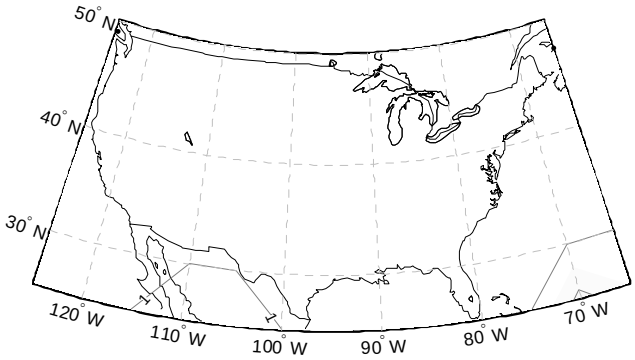

Figure 8. Availability Map For Dual-Frequency GPS and Iridium

APPENDIX I. REFINED IONOSPHERIC ERROR MODEL IN KALMAN FILTER AND BATCH IMPLEMENTATIONS

The ionospheric error model is included in the estimation and detection algorithms by state augmentation. Both a Kalman filter (KF) and a weighted least-squares batch (LSB) implementation are simulated. The KF is derived in the perspective of future real time applications.

For the KF implementation, the state propagation equation from epoch k to $k+1$ is written in the form:

$$^{KF}\mathbf{x}_{k+1} = \mathbf{\Phi}_k \, ^{KF}\mathbf{x}_k + \mathbf{w}_k$$

where $^{KF}\mathbf{x}$ is the state vector, $\mathbf{\Phi}$ is the process matrix and $\mathbf{w}$ is the process noise vector. The ionospheric error parameters ^{s}VIB and ^{s}VIG are assumed constant, so that elements of $\mathbf{\Phi}$ corresponding to these states form an identity matrix, and the corresponding elements in $\mathbf{w}$ zero. Now at epoch k where d_{IPP} exceeds $d_{IPP,MAX}$, the process equation for ^{s}VIB and ^{s}VIG changes to:

$$\begin{bmatrix} \vdots \\ VIB \\ VIG \\ \vdots \end{bmatrix}_{k+1} = \begin{bmatrix} \ddots & & & \\ & 1 & d_{IPP,0:k} & \\ \cdots & 0 & 0 & \cdots \\ & \vdots & \vdots & \end{bmatrix}_k \begin{bmatrix} \vdots \\ VIB \\ VIG \\ \vdots \end{bmatrix}_k + \begin{bmatrix} \vdots \\ 0 \\ VIG_N \\ \vdots \end{bmatrix}_k$$

with $VIG_N \sim \mathrm{N}\left(0, \sigma^2_{VIG}\right)$. The ^{s}VIB value has been updated, such that:

$$VIB_{k+1} = VIB + d_{IPP,0:k} VIG \, .$$

In the case of the LSB implementation, a new state is allocated for each new parameter, and prior knowledge for the error states must also be provided. Consider three carrier phase measurements ϕ at epochs k to $k+2$ (the d_{IPP} limit is exceeded between k and $k+1$), with measurement noise $\varepsilon_{\phi,k}$ $\left(\varepsilon_{\phi,k} = \varepsilon_{M-\phi,k} + \nu_{RN-\phi,k}\right)$. Elements of the measurement equation 6 corresponding to ionospheric states become:

$$\begin{bmatrix} \cdots & \phi_k & \phi_{k+1} & \phi_{k+2} & \cdots \end{bmatrix}^T$$

$$= \begin{bmatrix} \cdots & & & \vdots & \cdots \\ & {}^{s}ob_{I,k} & {}^{s}ob_{I,k} d_{IPP,0:k} & 0 & \cdots \\ & {}^{s}ob_{I,k+1} & {}^{s}ob_{I,k+1} d_{IPP,0:k} & {}^{s}ob_{I,k+1} d_{IPP,k+1:k+1} & \\ & {}^{s}ob_{I,k+2} & {}^{s}ob_{I,k+2} d_{IPP,0:k} & {}^{s}ob_{I,k+2} d_{IPP,k+1:k+2} & \\ \cdots & & & & \cdots \end{bmatrix} \begin{bmatrix} \vdots \\ VIB \\ VIG \\ VIG_N \\ \vdots \end{bmatrix}$$

$$+ \begin{bmatrix} \cdots & \varepsilon_{\phi,k} & \varepsilon_{\phi,k+1} & \varepsilon_{\phi,k+2} & \cdots \end{bmatrix}^T$$

APPENDIX II. CODE AND CARRIER OBSERVATION AND MEASUREMENT NOISE COVARIANCE MATRICES

First, a state space representation of vector ${}^{s}\boldsymbol{\varphi}$ (${}^{s}\boldsymbol{\varphi} = [\,{}^{s}\phi_{k_O} \quad \cdots \quad {}^{s}\phi_{k_F}\,]^T$) is realized based on equation 2. Error parameters and their dynamic models are incorporated by state augmentation. Let $\mathbf{0}_{n\times m}$ be a $n \times m$ matrix of zeros. State coefficients are arranged in matrices that are needed in later steps, so that for satellite s:

$$ {}^{s}\mathbf{G} = \begin{bmatrix} {}^{s}\mathbf{g}_{k_O}^T & & \mathbf{0}_{1\times 4} \\ & \ddots & \\ \mathbf{0}_{1\times 4} & & {}^{s}\mathbf{g}_{k_F}^T \end{bmatrix}, \quad {}^{s}\Delta\mathbf{t} = \begin{bmatrix} 0 & \Delta t_{k_1} & \cdots & \Delta t_{k_F} \end{bmatrix}^T, $$

$$ {}^{s}\mathbf{ob}_T = \begin{bmatrix} {}^{s}ob_{T,k_O} & \cdots & {}^{s}ob_{T,k_F} \end{bmatrix}^T, $$

$$ {}^{s}\mathbf{c}_T = \begin{bmatrix} 0 & {}^{s}ob_{T,k_1} \cdot c_{T,k_1} & \cdots & {}^{s}ob_{T,k_F} \cdot c_{T,k_F} \end{bmatrix}^T, $$

$$ {}^{s}\mathbf{ob}_I = \begin{bmatrix} {}^{s}ob_{I,k_O} & \cdots & {}^{s}ob_{I,k_F} \end{bmatrix}^T \text{ and} $$

$$ {}^{s}\mathbf{c}_I = \begin{bmatrix} 0 & {}^{s}ob_{I,k_1} \cdot {}^{s}d_{IPP,k_1} & \cdots & {}^{s}ob_{I,k_F} \cdot {}^{s}d_{IPP,k_F} \end{bmatrix}^T. $$

Carrier phase observations for all n_S Iridium and GPS satellites are then stacked together:

$$ \boldsymbol{\varphi} = \begin{bmatrix} {}^{1}\boldsymbol{\varphi}^T & \cdots & {}^{n_S}\boldsymbol{\varphi}^T \end{bmatrix}^T. $$

The carrier phase measurement equation is written in the form of equation 5:

$$ \boldsymbol{\varphi} = \mathbf{H}_{\boldsymbol{\varphi}}\mathbf{x} + \mathbf{v}_{\boldsymbol{\varphi}}, $$

The carrier phase observation matrix $\mathbf{H}_{\boldsymbol{\varphi}}$ is constructed by blocks:

$$ \mathbf{H}_{\boldsymbol{\varphi}} = \begin{bmatrix} \mathbf{G} & \mathbf{B_N} & \mathbf{B_{ECB}} & \mathbf{B_{ECG}} & \mathbf{B}_{ZTD} & \mathbf{B}_{\Delta n} & \mathbf{B_{VIB}} & \mathbf{B_{VIG}} \end{bmatrix} $$

Each block corresponds to a vector of state parameters, and contains coefficients for all spacecraft, for the entire sequence of measurements. Let $n_K(s)$ be the number of samples for satellite s (which generally differs for Iridium SVs), and $\mathbf{1}_{n\times 1}$ be a $n \times 1$ column-vector of ones:

$$ \mathbf{G} = \begin{bmatrix} {}^{1}\mathbf{G} \\ \vdots \\ {}^{n_S}\mathbf{G} \end{bmatrix}, \quad \mathbf{B_N} = \mathbf{B_{ECB}} = \begin{bmatrix} \mathbf{1}_{n_K(1)\times 1} & & 0 \\ & \ddots & \\ 0 & & \mathbf{1}_{n_K(n_S)\times 1} \end{bmatrix}, $$

$$ \mathbf{B_{ECG}} = \begin{bmatrix} {}^{1}\boldsymbol{\Delta}\mathbf{t} & & 0 \\ & \ddots & \\ 0 & & {}^{n_S}\boldsymbol{\Delta}\mathbf{t} \end{bmatrix}, \quad \mathbf{B}_{ZTD} = \begin{bmatrix} {}^{1}\mathbf{ob}_T \\ \vdots \\ {}^{n_S}\mathbf{ob}_T \end{bmatrix}, $$

$$ \mathbf{B}_{\Delta n} = \begin{bmatrix} {}^{1}\mathbf{c}_T \\ \vdots \\ {}^{n_S}\mathbf{c}_T \end{bmatrix}, \quad \mathbf{B_{VIB}} = -\begin{bmatrix} {}^{1}\mathbf{ob}_I & & 0 \\ & \ddots & \\ 0 & & {}^{n_S}\mathbf{ob}_I \end{bmatrix}, $$

$$ \text{and } \mathbf{B_{VIG}} = -\begin{bmatrix} {}^{1}\mathbf{c}_I & & 0 \\ & \ddots & \\ 0 & & {}^{n_S}\mathbf{c}_I \end{bmatrix}. $$

A measurement equation similar to equation 5 is established for the code-phase observation vector $\boldsymbol{\rho}$. In this case, the sign on the ionospheric coefficients $\mathbf{B_{VIB}}$ and $\mathbf{B_{VIG}}$ is positive. Also, the columns of ones in $\mathbf{B_N}$ corresponding to the cycle ambiguity vector $\mathbf{N}$ are replaced by zeros; this explains why state vectors $\mathbf{N}$ and $\mathbf{ECB}$ have to be distinguished, even though columns of $\mathbf{B_N}$ and $\mathbf{B_{ECB}}$ are linearly dependent for carrier phase measurements.

The complete sequence of code and carrier phase signals for all satellites over the smoothing interval are included into a batch measurement vector $\mathbf{z} = [\boldsymbol{\varphi}^T \quad \boldsymbol{\rho}^T]^T$. We obtain equation 6:

$$ \mathbf{z} = \mathbf{H}\mathbf{x} + \mathbf{v}. $$

The measurement noise vector $\mathbf{v}$ is utilized to introduce the time-correlated noise due to multipath modeled as a GMP. Its covariance $\mathbf{V}$ is block diagonal, and each block corresponds to observations from a same SV over time. Within each block, the time-correlation between two measurements originating from a same satellite s at sample times t_i and t_j is modeled as $\sigma^2_{M-\rho/\phi} \cdot e^{-\Delta t_{ij}/T_M}$, where $\Delta t_{ij} = |t_i - t_j|$. $\sigma^2_{RN-\rho}$ and $\sigma^2_{RN-\phi}$ are also added to the diagonal elements to account respectively for code-phase and for carrier phase uncorrelated receiver noise.

ACKNOWLEDGMENTS

The authors gratefully acknowledge the The Boeing Co. and the Naval Research Laboratory for sponsoring this work. However, the opinions expressed in this paper do not necessarily represent those of any other organization or person.

REFERENCES

[1] Danchik, R. "An Overview of Transit Development." *John Hopkins APL Technical Digest*. 19.1 (1998): 18-26.

[2] Rabinowitz, M., B. Parkinson, C. Cohen, M. O'Connor, and D. Lawrence. "A System Using LEO Telecommunication Satellites for Rapid Acquisition of Integer Cycle Ambiguities." *Proceedings of ION/IEEE Position Location and Navigation Symposium*. Palm Springs, CA. (1998): 137-145.

[3] Brown, R. "A Baseline RAIM Scheme and a Note on the Equivalence of Three RAIM Methods." *NAVIGATION: Journal of the Institute of Navigation*. 39.4 (1992): 127-137.

[4] RTCA Special Committee 159. "Minimum Operational Performance Standards for Global Positioning System/Wide Area Augmentation System Airborne Equipment." *Document No. RTCA/DO-229C*. Washington, DC. (2001).

[5] Hansen, A., J. Blanch, T. Walter, and P. Enge. "Ionospheric Correlation Analysis for WAAS: Quiet and Stormy." *Proceedings of the Institute of Navigation GPS Conference*. Salt Lake City, UT. (2000).

[6] McGraw, G., T. Murphy, M. Brenner, S. Pullen, and A. Van Dierendonck. "Development of the LAAS Accuracy Models." *Proceedings of the Institute of Navigation GPS Conference*. Salt Lake City, UT. (2000): 1212-1223.

[7] RTCA Special Committee 159. "Minimum Aviation System Performance Standards for the Local Area Augmentation System (LAAS)." *Document No. RTCA/DO-245*. Washington, DC. (2004).

[8] Fossa, C., R. Raines, G. Gunsch, and M. Temple. "An Overview of the Iridium Low Earth Orbit (LEO) Satellite System." *Proceedings of the IEEE National Aerospace and Electronics Conference*. (1998): 152-159.

[9] Kidder, S., and T. Vonder Haar. "A Satellite Constellation to Observe the Spectral Radiance Shell of Earth." *Proceedings of the Conference on Satellite Meteorology and Oceanography.* (2004): 1-5.

[10] NSTB/WAAS T&E Team, William J. Hughes Technical Center. "Wide-Area Augmentation System Performance Analysis Report." *available online at http://www.nstb.tc.faa.gov/DisplayArchive.htm.* Atlantic City, NJ: Reports No. 5-23. (2003-2008).

[11] Olynik, M., M. G. Petovello, M. E. Cannon, and G. Lachapelle. "Temporal Variability of GPS Error Sources and Their Effect on Relative Positioning Accuracy." *Proceedings of the Institute of Navigation NTM 2002*. San Diego, CA. (2002).

[12] Bae, T. S. "Near-Real-Time Precise Orbit Determination of Low Earth Orbit Satellites Using an Optimal GPS Triple-Differencing Technique." *PhD Dissertation*. Columbus, OH: Ohio State University. (2006).

[13] Misra, P., and P. Enge. *Global Positioning System: Signals, Measurements, and Performance*, *Second Edition*. Lincoln, MA: Ganga-Jamuna Press. (2006).

[14] DeCleene, B. "Defining Pseudorange Integrity - Overbounding." *Proceedings of the Institute of Navigation GPS Conference*. Salt Lake City, UT. (2000): 1916-1924.

[15] van Graas, F. *personal communication*. (2007).

[16] Lee, J., S. Pullen, S. Datta-Barua, and P. Enge. "Assessment of Nominal Ionosphere Spatial Decorrelation for GPS-Based Aircraft Landing Systems." *Proceedings of the IEEE/ION Position Location and Navigation Symposium*. San Diego, CA. (2006).

[17] Assistant Secretary of Defense for Command, Control, Communications and Intelligence. "Global Positioning System Standard Positioning Service Performance Standard." *available online at http://www.navcen.uscg.gov/GPS /geninfo/2001SPSPerformanceStandardFINAL.pdf.* Washington, DC. (2001).

[18] Cohen, C., B. Pervan, and B. Parkinson. "Estimation of Absolute Ionospheric Delay Exclusively through Single-Frequency GPS Measurements." *Proceedings of the Institute of Navigation GPS Conference*. Albuquerque, NM. (1992).

[19] Blanch, J. "Using Kriging to Bound Satellite Ranging Errors Due to the Ionosphere." *PhD Dissertation*. Stanford, CA: Stanford University. (2003).

[20] Tascione,T. *Introduction to the Space Environment. 2nd Ed.* Malabar, FL: Krieger Publishing Company. (1994).

[21] Crassidis, J., and J. Junkins. *Optimal Estimation of Dynamic Systems*. Boca Raton, FL: Chapman & Hall/CRC. (2004).

[22] Sturza, M. "Navigation System Integrity Monitoring Using Redundant Measurements." *NAVIGATION: Journal of the Institute of Navigation*. 35.4 (1988): 69-87.